Theory and Modeling of the Binding in Cationic Transition-Metal−Benzene Complexes

Chia-Ning Yang and Stephen J. Klippenstein*

Chemistry Department, Case Western Reserve University, Cleveland, Ohio 44106-7078

Received: August 31, 1998; In Final Form: December 18, 1998

Binding energies are estimated for the complexes of benzene with the first-row transition-metal ions ($M^+ = Ti^+-Cu^+$) via both kinetic modeling and quantum chemical simulation. A variational transition-state theory model implementing an ion−quadrupole plus ion-induced dipole potential is employed in the modeling of the kinetic data for the collision-induced dissociation of these complexes. For Cr^+, a global potential is generated for its interaction with benzene and radiative association experiments are also modeled. Implementation of this potential in the transition-state analyses indicates only minor anharmonicity effects for the complex state density near the dissociation threshold and negligible deviation from the long-range potential-based predictions for the transition-state partition functions. Theoretical optimized geometries, binding energies, and vibrational frequencies are determined with the B3LYP (Becke-3 Lee−Yang−Parr) density functional. The V^+, Ni^+, and Fe^+ complexes are found to have modest Jahn−Teller-induced boat-shaped distortions of the benzene ligand. The quantum chemical and kinetic modeling based estimates for the binding energies are in reasonable agreement.

I. Introduction

Various methods for extracting/estimating binding energies for ion−molecule complexes from experimental kinetics measurements rely upon estimates for the dissociation and/or association kinetics. Of particular interest here are methods based on the modeling of collision-induced dissociation[1−2] and radiative association experiments.[3−4] In the former experiment, the observed dissociation threshold corresponds to the energy at which the ion dissociates on a time scale of 10^{-4} s. The kinetic shift, which corresponds to the difference between this observed threshold and the true 0 K threshold, grows rapidly with increasing molecular size. As a result, accurate kinetic estimates are of great importance when applying this methodology to the dissociation of large species.

Radiative association experiments observe the rate at which stabilized complexes are formed via radiative emission from the initially formed association complex. The kinetics of this radiative stabilization are competing with the dissociation of the complex back to the separated reactants as described in detail in ref 4. For very small species, the stabilization probability is so low as to make useful measurements difficult. In contrast, for very large species, the stabilization probability approaches unity and then the kinetics becomes independent of binding energy. Thus, the determination of binding energies from the modeling of the radiative association kinetic data is most effective for intermediate-sized species such as the metal−benzene cationic complexes of interest here. In this range, an accurate modeling of the kinetics generally requires estimates for the back dissociation rate constants.

In a recent collision-induced dissociation study, Armentrout and co-workers employed standard rigid-rotor harmonic-oscillator (RRHO) transition-state theory (TST) models in the estimation of the kinetic shifts (and thereby binding energies) for the complexes of benzene with first-row transition-metal cations.[5] The estimated kinetic shifts in this study were quite substantial, the largest being 10 kcal/mol. They also obtained valuable qualitative estimates of the uncertainty in the estimated kinetic shifts by contrasting loose and tight models for the transition state.

Recent theoretical advances allow for the implementation of important improvements in the modeling of such kinetic shifts. In particular, the focus of the present study is on the implementation of density functional theory estimates for the molecular properties within a variational transition-state theory (VTST) model for the kinetics. Quantum chemical estimates for the binding energies of the metal−benzene cations have been obtained previously.[6−8] However, these studies do not provide the requisite vibrational frequencies for the present study. Density functional theory generally provides reasonable estimates for these frequencies at a relatively modest computational cost. The implementation of these vibrational frequencies within a fundamentally based VTST approach should provide a firmer foundation for the kinetic shift corrections.

The present VTST evaluations generally employ a long-range ion-induced dipole plus ion−quadrupole potential. To test the validity of this long-range form for the potential, we have examined the interaction between benzene and Cr^+ in detail via a series of ab initio calculations spanning a range of separation and orientation. A spline fit of this ab initio data then provides an analytic potential. A comparison of the VTST results obtained while implementing this ab initio based potential with those obtained for the long-range potential illustrates the general validity of the long-range potential.

The Cr cation is chosen for these detailed evaluations for a variety of reasons. Firstly, the electronic configuration of Cr^+ is well defined and unchanging during reaction. As a result, the ab initio quantum chemical evaluations are relatively straightforward and reliable. This constancy of the electronic configuration also means that the theoretical predictions for the kinetics are more reliable since there is no need to estimate rate constants for electronic transitions. Furthermore, the availability of radiative association data for this reaction[9] provides a valuable opportunity for testing the consistency of the two different kinetic modeling schemes. Finally, the comparatively large

10.1021/jp9835770 CCC: $18.00
Published on Web 02/06/1999

metal−ligand bond length and correspondingly low metal−ligand vibrational frequencies suggest that anharmonic effects might be quite large for this complex. The generation of a global analytic potential for the metal−ligand interaction allows for the quantitative investigation of such effects.

II. Quantum Chemistry Methodology

Nonlocal density functional theory (DFT) was employed in the determination of the optimized structures and infrared spectral properties for each of the $M(C_6H_6)^+$ complexes, the metal cations ($M^+ = Ti^+-Cu^+$), and the benzene ligand. These determinations employed the B3-LYP (Becke-3 Lee−Yang−Parr) hybrid functional,[10] the 6-311+G(d) basis set for the metal ions, and the 6-31G* basis set for the C and H atoms.[11] The metal basis set includes one set of f polarization functions. All the quantum chemistry calculations described here were performed with the Gaussian94 quantum chemistry software.[11]

The quantum chemical binding energies reported below incorporate corrections for basis-set superposition errors (BSSE) obtained on the basis of a recently described scheme of Xantheas.[12] This scheme adds a correction for geometrical relaxation effects to the standard counterpoise correction, thereby yielding equivalent values for the corrected and uncorrected complete basis-set limits. For the present systems, the net basis-set superposition corrections ranged from 2.7 to 3.8 kcal/mol while the relaxation energies varied from 0.4 to 2.1 kcal/mol.

The $Cr^+\cdots C_6H_6$ interaction potential was evaluated with second-order Møller Plesset (MP2) perturbation theory[13] instead of density functional theory due to unphysical behavior at large separations for the B3-LYP functional. The combination of the 6-311+G(d) basis for the metal and the 6-31G* basis for the ligand was again employed. The MP2 binding energy is only 1.4 kcal/mol lower than the B3LYP value, and the MP2 metal-ligand stretching and bending force constants are within 5% of the B3LYP values. Thus, for Cr^+, MP2-level calculations would appear to provide a reasonable description of the interaction potential.

In these interaction energy calculations, the benzene structure was held fixed at the optimized structure for free benzene. The relaxation energy is only 0.7 kcal/mol, and its neglect should be insignificant in the present considerations of anharmonicity effects for the interfragment modes. The energies were evaluated on various grids of $M^+\cdots$benzene distances and orientations. These grids employed the spherical polar coordinates (R,θ,ϕ). The origin of these coordinates is the center of the benzene ring, and the perpendicular to the benzene plane corresponds to the z-axis with $\theta = 0$. The x-axis ($\theta = 90°$, $\phi = 0$) is taken to lie along a CH bond. The midpoint of a CC bond then lies at $\theta = 90°$, $\phi = 30°$. With these definitions, the potential has periodicities of 180° in θ and 60° in ϕ, and is symmetric about $\theta = 90°$ and about $\phi = 30°$. Furthermore, the potential is only weakly dependent on ϕ for values near the optimum geometry for any R, and so simply considering $\phi = 0$ and 30° was deemed sufficient. At short separations, a grid of 5° was employed for θ in the range from 0 to 15° and a 7.5° grid was employed for θ above 15°. For separations beyond $R = 4$ Å, a sparser θ grid (consisting of $\theta = 0°$, 5°, and then a 15° spacing from 15° up to 90°) was employed since the anisotropy of the potential is greatly decreased. For the R grid, a 0.1 Å spacing was employed for R's ranging from 1.4 to 2.6 Å, while a 0.2 Å grid was employed for $R = 2.6$ to 7.0 Å and a 0.5 Å grid for $R = 7.0$ to 10.0 Å. An analytic potential is obtained from these grids via spline fits in R and θ and a Fourier expansion in ϕ.

III. Transition-State Theory Methodology

We describe here the methodology employed in the determination of the energy E and angular momentum J resolved dissociation rate constants. Such dissociation rate constants are an integral part of the kinetic modeling of both the collision-induced dissociation and radiative association experiments. The transition-state number of states, $N^\dagger_{EJ}$, was evaluated according to a version of variational transition-state theory which employs an assumed decoupling of the vibrational modes of the benzene ligand from the remaining modes.[4,14] The former modes have been termed the conserved modes due to their near invariance during the reaction process, while the latter have been termed the transitional modes. The conserved modes are treated as quantum harmonic oscillators, and their contribution is evaluated via a Beyer−Swinehart[15] direct counting. The transitional mode contribution is obtained via the Monte-Carlo evaluation of a classical phase space integral representation which properly conserves energy and total angular momentum within this subset of modes.

A long-range anisotropic ion-induced dipole plus ion−quadrupole potential was generally employed in the evaluation of these phase space integrals:

$$V_{lr} = -\frac{q^2}{2R^4}(\alpha_{||}\cos^2\theta + \alpha_\perp \sin^2\theta) + \frac{qQ\,(3\cos^2\theta - 1)}{2R^3} \tag{1}$$

For benzene, the components of the polarizability are $\alpha_{||} = 6.7$ Å^3 and $\alpha_\perp = 12.3$ Å^3 [16] while the quadrupole moment is −8.5 Debye Å.[17] For Cr^+, the ab initio based spline fit potential was also employed in the transition-state theory (TST) evaluations.

The variable reaction coordinate TST (VRC−TST) formalism employed here considers a variety of different forms for the transition-state (TS) dividing surface.[14,18] For the present $M^+\cdots C_6H_6$ case, any one dividing surface corresponds to a fixed distance r between the metal ion and a pivot point fixed to the frame of the benzene ligand. The pivot point is defined relative to the benzene center-of-mass by the vector **d** and corresponds to the point about which the benzene rotations occur. The number of available states $N_{EJ}(r,\mathbf{d})$ is then evaluated for a grid of both **d** and r with the TS number, $N^\dagger_{EJ}$, being given by the minimum over this grid.

The density of state, ρ_{EJ}, for the complex was also generally evaluated on the basis of rigid-rotor harmonic-oscillator estimates. However, the low frequencies observed for the metal−benzene modes, together with the strong long-range attraction of the metal ions to the ligand, suggests that there may be important anharmonic and/or nonrigidity effects for this density of states. Such effects are explicitly considered here for the Cr^+ case making use of the MP2 ab initio based spline fit potential.

In the examination of these effects, we again implement an assumed decoupling of the conserved and transitional modes

$$\rho_{EJ} = \int d\epsilon \rho_c(E-\epsilon)\rho_t(\epsilon,J) \tag{2}$$

where ρ_c is the state density for the conserved modes and ρ_t is that for the transitional modes. The conserved mode state density is again evaluated via a direct count over the quantum harmonic energy levels. For the transitional modes, an approximate quantum nonrigid/anharmonic estimate $\rho_t^{q,a}(E,J)$ is obtained via the evaluation of (i) a classical phase-space integral-based density $\rho_t^{c,a}(E,J)$ which properly conserves angular momentum and employs the full anharmonic potential, (ii) a quantum rigid-rotor harmonic oscillator (RRHO) estimate, $\rho_t^{q,h}(E,J)$, and (iii)

TABLE 1: B3LYP Structural Results for $M(C_6H_6)^+$

metal	state	R_{M-Ring}[a]	R_{CC}[b]	θ_1[c]	θ_2[d]
Ti	$^4A_1(3de_2^2 3da_1^1)$	1.883(2.059)	1.418	−0.5	
V	$^5B_2(3da_1^2 3da_2^1 3db_1^1)$	1.929(1.964)	1.409,1.416	−1.4,−2.0	2.6
Cr	$^6A_1(3de_2^2 3da_1^1 3de_1^2)$	2.104(2.110)	1.410	−1.1	
Mn	$^7A_1(3de_2^2 3da_1^1 3de_1^2 4s^1)$	2.360(2.300)	1.407	−0.5	
Fe	$^4A_1(3da_1^4 3da_2^1 3db_1^1 3db_2^1)$	1.826	1.407,1.419	−1.1,−4.1	4.7
Fe	$^4A_1(3de_2^4 3da_1^1 3de_1^2)$	1.665(1.830)	1.422	1.2	
Fe	$^6A_1(3da_1^3 3da_2^1 3db_1^1 3db_2^1 4sa_1^1)$	2.207(2.153)	1.407,1.408	−0.2,−0.2	0.9
Co	$^3A_1(3de_2^4 3da_1^2 3de_1^2)$	1.663(1.854)	1.418	1.2	
Ni	$^2B_2(3da_1^4 3da_2^2 3db_1^2 3db_2^1)$	1.715(1.750)	1.411,1.418	−0.5,−0.9	2.7
Cu	$^1A_1(3de_2^4 3da_1^2 3de_1^4)$	1.848(1.852)	1.414	−0.6	

[a] Metal to ring center distance in Å. Numbers in parentheses are MCPF/DZP results from ref 6. [b] CC bond length in Å. For Jahn−Teller-distorted species, the first value corresponds to bonds between the 4-fold degenerate C atoms and the second to the other CC bond. [c] Out-of-plane bending angle for the H atom in degrees. Positive values correspond to bending toward the metal cation. Where there is more than one value, the first is for the 4-fold degenerate H atoms while the second is for the 2-fold degenerate H atoms. [d] Out-of-plane bending angle in degrees for the 2-fold degenerate C atoms in the Jahn−Teller-distorted structures. Positive values correspond to bending toward the metal cation.

a classical RRHO estimate, $\rho_t^{c,h}(E,J)$:[19−21]

$$\rho_t^{q,a} \approx \rho_t^{q,h} \frac{\rho_t^{c,a}}{\rho_t^{c,h}} \tag{3}$$

The quantum and classical RRHO densities are obtained from standard expressions. The procedures employed in the evaluation of the classical nonrigid/anharmonic state density are outlined in the Appendix. A related procedure for evaluating anharmonic state densities was employed in ref 22.

For each of the reactions, symmetry numbers of 6, 12, and 12 were employed in the VRC−TST models for the density of states of the complex, the number of states at the transition state, and the partition function for the fragments, respectively. The choice of 12 as the symmetry number for the transition state is appropriate in light of the inclusion of the contributions from both faces in the evaluation of the transition state number of states. For the RRHO models of ref 5, the TS is assumed to be similar to the complex. Thus, symmetry numbers of 6 and 6 were employed for the density of states of the complex and the number of states for the transition state in our replication of those models.

IV. Quantum Chemical Results

Structures and Energetics. A detailed description of the electronic factors involved in the bonding between benzene and the transition-metal cations has been provided by Bauschlicher et al. in their modified couple pair functional (MCPF) based ab initio quantum chemical study.[6] Thus, the numerical values obtained with the present B3LYP DFT calculations are only briefly reviewed, recalling that the present focus is on the efficient determination of meaningful estimates for the vibrational properties.

The B3LYP optimized structures obtained for each of the metal benzene cations are reported in Table 1. The partial occupation of orbitals which are degenerate in C_{6v} symmetry for the V^+, Ni^+, $^6Fe^+$ and $^4Fe^+[3da_1^4 3da_2^1 3db_1^1 3db_2^1(C_{2v}) \leftrightarrow 3de_2^3 3da_1^2 3de_1^2(C_{6v})]$ complexes results in modest boat-shaped Jahn−Teller distortions to C_{2v} symmetry for the C ring framework, with the 2-fold C atoms bending toward the metal ion with increased CC bond lengths. This distortion also leads to a strong coupling of the metal−ligand bending modes with some of the lowest frequency ligand modes. The other complexes do not have such partially filled degenerate orbitals and were found to have C_{6v} symmetry.

The interaction with the metal ion results in a modest increase in the CC bond lengths from the free benzene value of 1.397 Å. This deviation, which ranges from 0.010 to 0.037 Å, tends to increase with decreasing separation between the metal and the ring. The CH bond lengths are more constant, decreasing by 0.002 Å or less in the complexation process. The bending of the H atoms relative to the plane of the C ring framework is always small and generally away from the metal cation.

Most of the metal ring separations calculated at the B3LYP level are in reasonable agreement with the corresponding MCPF/DZP estimates of ref 6, generally differing by 0.06 Å or less. However, for three of the complexes, (Ti^+, Co^+, and the $^4Fe^+$ complex with an orbital occupation of $3de_2^4 3da_1 3de_1^2$), the differences are much larger, 0.18 ± 0.01 Å. Notably, these three complexes are the only ones having an electronic configuration for the complex which does not correlate with that of the ground-state ions. Instead, that for Ti^+ correlates with a state which is 80% ^4F and 20% ^4P, that for Co^+ correlates with a state which is 80% ^3F and 20% ^3P, and that for Fe^+ correlates with a state which is 20% ^4F and 80% ^4P.[23] The differences in these bond lengths, together with the deviations in the binding energies for the $^4Fe^+$ states noted below, suggests that the B3LYP and MCPF methods provide a quite different treatment of the F to P excitation.

The B3LYP estimated binding energies for the ground-state to ground-state dissociation process are reported in Table 2. Also reported therein are the total BSSE and its component due to fragment relaxation. The variation in the total BSSE arises primarily from the variation in the fragment relaxation component, which tends to increase with decreasing metal−ring separation. The binding energies show a similar trend, although there are more and stronger variations.

The average spin-squared values reported in Table 2 indicate that there is very little spin contamination for each of the states. Only that for the $^4Fe^+$ state with a $3de_2^4 3da_1 3de_1^2$ orbital occupation has a spin contamination which exceeds 1%, and even that is only 3%. The absence of any significant spin contamination suggests that the B3LYP functional likely provides an adequate treatment of the multireference nature of these open-shell wavefunctions.

For comparison purposes, Bauschlicher et al.'s MCPF/DZP based estimates[6] for the binding energies are also reported in Table 2. The two sets of purely quantum chemical results are generally in very good agreement, differing by 2.0 kcal/mol or less. This good agreement further validates the use of the B3LYP density functional method for this type of system.

TABLE 2: B3LYP Energetics[a] for $M(C_6H_6)^+$

metal	state	R_{M-Ring}[b]	ΔE_{relax}[c]	BSSE[d]	$\langle S^2\rangle$[e]	D_0[f]	D_e[g]
Ti	$^4A_1(3de_2^2 3da_1^1)$	1.883	1.3	3.7	3.753	59.3	60.6
						56.9[g]	**62.8**
V	$^5B_2(3da_1^2 3da_2^1 3db_1^1)$	1.929	1.2	3.8	6.005	49.7	51.1
Cr	$^6A_1(3de_2^2 3da_1^1 3de_1^2)$	2.104	0.7	3.2	8.754	38.9	37.4
Mn	$^7A_1(3de_2^2 3da_1^1 3de_1^2 4sa_1^1)$	2.360	0.4	2.7	12.003	34.5	35.1
Fe	$^4A_1(3da_1^4 3da_2^1 3db_1^1 3db_2^1)$	1.826	1.7	3.5	3.782	57.2	
						51.5	
Fe	$^4A_1(3de_2^4 3da_1^1 3de_1^2)$	1.665	2.1	3.7	3.834	45.6	47.6
						39.9	**51.1**
Fe	$^6A_1(3da_1^3 3da_2^1 3db_1^1 3db_2^1 4sa_1^1)$	2.207			8.756	40.9	41.7
Co	$^3A_2(3de_2^4 3da_1^2 3de_1^2)$	1.663	1.5	3.8	2.024	61.2	62.6
Ni	$^2B_2(3da_1^4 3da_2^2 3db_1^2 3db_2^1)$	1.715	1.4	3.7	0.755	59.9	59.3
Cu	$^1A_1(3de_2^4 3da_1^2 3de_1^4)$	1.848	0.9	3.4	0	51.7	51.1

[a] All energies are in kcal/mol, and the binding energies are relative to the ground state of the separated ion and benzene. [b] Metal to ring center distance in Å. [c] Contribution to BSSE from fragment relaxation. [d] Total BSSE. [e] B3LYP estimated dissociation energy including zero-point and BSSE corrections. [f] Average spin squared for the complex. [g] MCPF/DZP estimated dissociation energy from ref 6. [h] For the $^4Ti^+$ and $^4Fe^+$ states, the bold numbers correspond to binding energies evaluated by adding the experimental promotion energy to the theoretical estimate for the spin conserving dissociation process. In contrast, the primary entries denote the purely theoretical energy for the ground-state to ground-state dissociation process.

For the $^4Ti^+$ and $^4Fe^+$ states, the binding process involves a 4s to 3d promotion from the free ion to the complex. In this instance, a generally better estimate for the binding energy may be obtained from the combination of quantum chemical estimates for the diabatic (metal ion state conserving) binding energy with the known experimental promotion energy.[24] The B3LYP functional actually estimates the ^4F $Ti^+(d^3)$ and ^4F $Fe^+(d^7)$ states to be more stable than the corresponding $^4Ti^+(d^2s)$ and $^6Fe^+(d^6s)$ ground states. In contrast, MCPF theory slightly underestimates the stability of these two excited states. For Ti^+, this results in a comparatively large difference of 5.9 kcal/mol between the two improved estimates for the binding energies.

For Fe, the situation is more complex. For the $Fe^+(3de_2^4 3da_1^1 3de_1^2)$ configuration there is an unreasonably large difference of 11.2 kcal/mol between the adjusted B3LYP and MCPF results. However, the present B3LYP calculations suggest that the ground $^4Fe(C_6H_6)^+$ state corresponds to a $3de_2^3 3da_1^2 3de_1^2$ orbital occupation in C_{6v} symmetry (which correlates to a $3da_1^4 3da_2^1 3db_1^1 3db_2^1$ configuration in the Jahn−Teller distorted C_{2v} geometry). For this state, the adjusted B3LYP binding energy of 51.5 kcal/mol agrees very well with that for the MCPF calculated ground state (51.1 kcal/mol).

The smaller B3LYP binding energy for the $3de_2^4 3da_1^1 3de_1^2$ $^4Fe^+$ state suggests that the B3LYP ^4F to ^4P splitting is substantially greater than the MCPF value. A similar difference for the Ti^+ ^4F to ^4P splittings may also provide an explanation for the relatively large deviation for the adjusted Ti results. Interestingly, MP2 calculations at the B3LYP optimized geometries predict adjusted binding energies for the sextet, quartet (C_{6v}), and quartet (C_{2v}) $Fe(C_6H_6)^+$ states, which are in reasonable agreement with the B3LYP values, being 1.6, 5.7, and 3.3 kcal/mol greater, respectively (prior to any BSSE corrections). Related calculations for H_2O, C_2H_2, and C_2H_4 ligands show a good correlation between adjusted B3LYP and coupled-cluster calculations with a perturbative inclusion of triple excitations [CCSD(T)].[25] In particular, for the lowest sextet states, the deviations are 0.5, 1.9, and 2.9 kcal/mol, respectively, while for the lowest quartet states the deviations are 2.4, 5.9, and 5.3 kcal/mol. This agreement relies on, and verifies, the use of the experimental spin splittings since the B3LYP values are greater than the CCSD(T) values for each of these states, even after the adjustments.

Interaction Potential for $Cr(C_6H_6)^+$. Various contributions to the interaction potential are plotted in Figure 1 for motion of the Cr cation along the C_{6v} symmetry axis ($\theta = 0$) and in the benzene plane along the CC symmetry axis ($\theta = 90°$, $\phi = 0$). The MP2 ab initio quantum chemical potential is seen to agree closely with the long-range ion−quadrupole plus ion-induced dipole potential for separations of about 6−8 Å or greater. The ion−quadrupole interaction is a dominant component of the long-range potential throughout this range of separations. At large metal−ligand separations, the Cr cation prefers to be perpendicular to the benzene plane ($\theta = 0$) due to this dominance of the ion−quadrupole interaction.

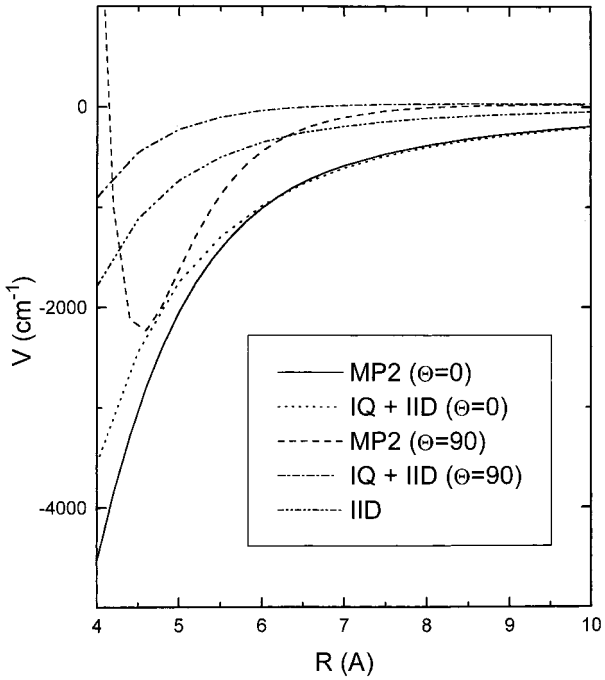

Figure 1. Plot of the R dependence of various contributions to the Cr^+−benzene interaction potential all for $\phi = 0$. The solid and dashed lines are the MP2 results for $\theta = 0°$ and 90°, respectively. The dot−dot−dashed line is for the ion-induced dipole interaction employing the isotropic average polarizability. The dotted and dot−dashed lines are for the ion−quadrupole plus anisotropic ion-induced dipole potential for angles of 0° and 90°, respectively.

A contour plot of the MP2-based potential for the interaction of benzene with Cr^+ is provided in Figure 2. This plot is for the Cr cation moving in the plane perpendicular to the benzene

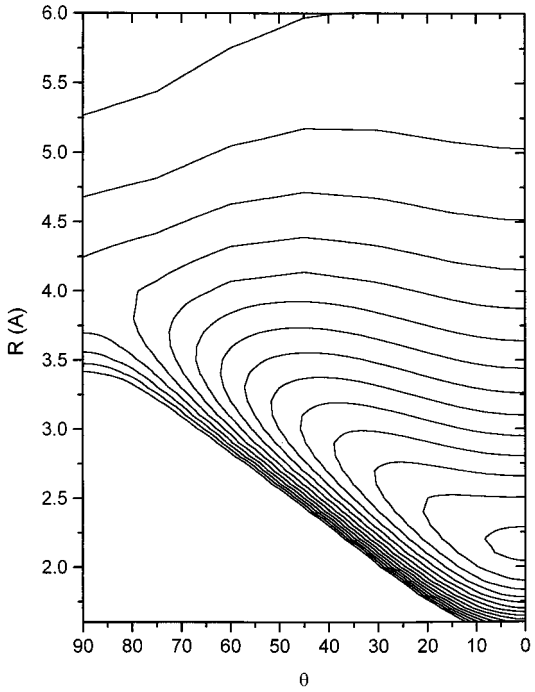

Figure 2. Contour plot of the MP2 calculated Cr^+−benzene interaction potential for $\phi = 30°$. The contour spacing is 1000 cm^{-1}. The contour at the top left is for −1000 cm^{-1}, while the lowest contour is near the bottom right with a value of −14 000 cm^{-1}.

plane with $\phi = 30°$. The corresponding plot for $\phi = 0°$ is qualitatively similar but becomes repulsive at slightly larger (e.g., 0.7 Å) separations for ϕ near 90°.

As the separation decreases below about 6.5 Å, the optimum θ gradually increases, reaching a maximum of about 45° near $R = 4.0$ Å. This change in the optimum orientation is a result of the increased importance of both the ion-induced dipole interactions (which favor $\theta = 90°$) and specific metal−ligand bonding interactions. As the separation decreases below 4.0 Å, the optimum orientation now gradually decreases, reaching a 0 value at $R = 2.38$ Å. The reasonably close proximity of this separation to the optimum unrelaxed separation for the complex ($R = 2.15$ Å) suggests that the estimated bending frequency will be strongly dependent on the optimum separation. In fact, for somewhat smaller basis sets, the equilibrium structure was actually of C_{2v} rather than C_{6v} symmetry as a result of the optimum separation moving out past the separation at which the transition to $\theta = 0$ occurs. Of course, at the separation where the transition from non-zero to zero values for the optimum θ occurs, the harmonic bending frequency is identically zero.

This strong dependence of the harmonic bending frequency on the separation distance provides further motivation for the anharmonic non-rigid-rotor-based evaluation of the density of states for the Cr^+ complex. Unfortunately, it also suggests that any quantum chemical estimate of the bending frequency (and correspondingly the contribution to the density of states for the complex) is somewhat uncertain due to the inherent difficulty of accurately determining the metal−ring separation.

Vibrational Properties. The B3LYP estimated vibrational frequencies and rotational constants for benzene and each of the metal benzene cation complexes are reported in Table 3. The metal to ligand stretching frequencies lie in the range from 165 to 311 cm^{-1}, while the corresponding bending frequencies lie in the range from 85 to 293 cm^{-1}. Aside from the Jahn−Teller-distorted complexes, there is only a weak perturbation of the free benzene modes in the complexes. Sample evaluations for Cr^+ indicated that inclusion of diffuse functions on the C's and diffuse and polarization functions on the H's has little effect on these vibrational properties.

Armentrout and co-workers estimated metal−ligand stretching and bending frequencies on the basis of SCF calculations (from Bauschlicher) for $Ag(C_6H_6)^+$.[5] Their frequencies are all lower than those estimated here, particularly the bending frequencies which were estimated to be nondegenerate and in the ranges from 14 to 20 and 50 to 66 cm^{-1}. The product of their two bending frequencies ranges from a factor of 8 to 90 below the current estimates, which might be expected to have a major impact on the kinetic modeling.

The low value for their frequencies is related to the above-mentioned dependence of the bending force constant on the variation of the optimum θ. At the SCF level for Ag−benzene cation, the optimum geometry is predicted to be of C_s symmetry with correspondingly low values for the bending frequencies. Subsequent MP2 level calculations suggest that the distance from Ag^+ to the ring center is much shorter (2.27 vs 2.56 Å) and that the $Ag(C_6H_6)^+$ complex is of C_{6v} symmetry.[26] As a result, one of the bending frequencies is predicted to be a factor of three greater than suggested at the SCF level.[26] The even shorter separations predicted for the present first-row transition-metal complexes lead to increases in both the bending and stretching force constants, which are considerably greater than estimated by Armentrout and co-workers on the basis of the variations in mass and binding energy.

Also reported in Table 3 are the IR absorption intensities for the $Cr(C_6H_6)^+$ complex since these intensities play an important role in the radiative association modeling. The dominant radiative modes are the 749 cm^{-1} mode with an intensity of 104 km/mol and the doubly degenerate mode at 1506 cm^{-1} with an intensity of 15 km/mol. The cubic scaling of the radiative emission rates with frequency results in a roughly equivalent contribution from these two modes. The intensities for these two dominant radiative modes were estimated to be a factor of 2 greater in the Hartree−Fock-based calculations of Lin and Dunbar.[9] Their calculations also differed in predicting metal−ligand frequencies, which were only about 60% of the present B3LYP estimates, due to a much greater optimized Cr^+ ring separation of 2.526 Å. Again, such differences may have a significant impact on the kinetic modeling.

V. Kinetics Results

A. Cr^+. *Density of States.* The ratio of the full phase-space integral-based estimate for the state density of the complex to the RRHO-based estimate is plotted as a function of energy for several values of the total angular momentum J in Figure 3. The range of J values plotted roughly corresponds to the range of J of importance in the radiative association modeling. The E values plotted range from well below the dissociation threshold of about 14 000 cm^{-1} to a maximum value which corresponds to a typical maximum excess E of importance in the modeling of the kinetic shifts for the collision-induced dissociation experiments. For J values near the typical most probable thermal value of 50, this ratio is only weakly dependent on both J and E, taking a value of 1.35 near the dissociation threshold and increasing to about 1.45 for an excess E of about 4000 cm^{-1}.

The increase in the ratio with both E and J is easily understood in terms of the variations in the average metal−ligand separation. In particular, the anharmonicity in the potential leads to a greater average separation for higher available energies. At these greater separations, both the rotational constants and the bending frequencies are smaller,

TABLE 3: B3LYP Vibrational Frequencies and Rotational Constants for $M(C_6H_6)^+$

metal	B[a]	ν[b]									
none	0.189	415	415	622	622	693	718	863	863	968	968
	0.189	1010	1020	1020	1068	1068	1185	1207	1207	1355	1388
	0.095	1531	1531	1655	1655	3179	3188	3188	3204	3204	3215
Ti	0.092	**293**[c]	**293**	**311**							
	0.086	414	414	615	615	635	775	888	888	962	962
	0.086	980	984	1025	1031	1031	1178	1178	1184	1351	1378
		1488	1488	1545	1545	3213	3218	3218	3228	3228	3234
V	0.093	**166**	**230**	**247**							
	0.081	225	411	544	613	659	763	892	912	976	985
	0.081	996	1008	1027	1032	1049	1188	1189	1190	1343	1380
		1493	1503	1567	1581	3215	3218	3221	3229	3234	3238
Cr	0.093	**94**	**94**	**188**							
	0.073	411	411	613	613	678	749	905	905	992	1000
	0.073	1000	1017	1028	1049	1049	1189	1201	1201	1328	1386
		1506	1506	1602	1602	3214	3220	3220	3230	3230	3236
		1.9[d]	*1.9*	*6.6*							
		0	*0*	*0*	*0*	*0*	*104*	*1.1*	*1.1*	*1.3*	*0*
		0	*0*	*0*	*2.8*	*2.8*	*0*	*0*	*0*	*0*	*0*
		15	*15*	*0*	*0*	*0*	*0*	*0*	*3.2*	*3.2*	*0.03*
Mn	0.094	**99**	**99**	**165**							
	0.063	377	377	611	611	677	754	914	914	1001	1014
	0.063	1014	1022	1036	1056	1056	1195	1208	1208	1349	1390
		1514	1514	1618	1618	3214	3220	3220	3230	3230	3236
^{4}Fe	0.093	**170**	**237**	**242**							
A^1	0.086	61	414	605	616	672	781	912	918	972	986
C_{2v}	0.085	989	1014	1030	1032	1049	1168	1189	1197	1336	1381
		1493	1502	1527	1595	3218	3221	3225	3232	3235	3239
^{4}Fe	0.093	**255**	**255**	**298**							
A_1	0.089	411	411	632	632	680	786	889	889	981	997
C_{6v}	0.088	997	1011	1029	1029	1062	1180	1180	1189	1369	1425
		1425	1481	1481	1546	3227	3231	3231	3239	3239	3244
Co	0.092	**250**	**250**	**283**							
	0.092	411	411	622	622	668	798	916	916	985	989
	0.092	992	992	1032	1038	1038	1170	1188	1188	1300	1377
		1492	1492	1571	1571	3221	3228	3228	3237	3237	3242
Ni	0.093	**147**	**194**	**240**							
	0.089	189	411	543	618	678	779	906	924	989	990
	0.088	1008	1017	1033	1033	1050	1189	1191	1191	1336	1381
		1493	1503	1576	1591	3223	3227	3229	3237	3241	3245
Cu	0.093	**85**	**85**	**200**							
	0.080	408	408	616	616	688	765	914	914	992	1004
	0.080	1004	1019	1033	1045	1045	1188	1200	1200	1319	1385
		1502	1502	1598	1598	3220	3226	3226	3235	3235	3241

[a] Rotational constants in cm^{-1}. [b] Vibrational frequencies in cm^{-1}. [c] The first two bold frequencies denote the metal−ligand bending modes, while the last bold frequency denotes the metal−ligand stretching mode. [d] For the Cr complex, the infrared intensities in km/mol are given in italics in the same order as the vibrational frequencies.

leading to an increased state density relative to the RRHO estimate. The increase in the average rotational energy with decreasing separation also leads to a greater average separation for higher J values.

These anharmonicities were incorporated in the VRC−TST modeling of both the collision-induced dissociation and radiative association experiments for Cr^+. The similarity of the structures and vibrational frequencies for Mn^+ led us to include an equivalent anharmonicity correction for Mn^+. For the remaining cations, the smaller metal to ring separations and larger frequencies led us to assume that the anharmonicity correction is negligible.

Dissociation Rate Constants. Various estimates for the energy dependence of the dissociation rate constant are plotted in Figure 4. The VRC−TST results are for the most probable J of 50, while the RRHO−TST results incorporate the rotational partition function correction factor according to the method of Waage and Rabinovitch[27] as described in refs 1 and 5. Averaging over the thermal distribution of J in the VRC−TST calculations provides a result which differs negligibly from that for the average J.

Interestingly, on the scale of the plot, the variable reaction coordinate TST (VRC−TST) results obtained for the full potential are essentially identical to those obtained when employing just the ion-induced dipole potential. At low energies, these VRC−TST results are similar to the loose TS results of Armentrout and co-workers. At higher energies, the VRC−TST results gradually move toward the tight TS results. This variation from the loose TS limit to the tight TS limit is indicative of the changing location of the TS as the energy increases. In particular, the TS separation decreases from 30 Å at an excess energy of 100 cm^{-1} to 12 Å at 1000 cm^{-1} and then 8 Å at an excess E of 6000 cm^{-1}. Concomitant with this decreasing separation is an increase in the effective bending frequency for the metal−ligand modes and the effective rotational constants.

Various different forms for the reaction coordinate were considered in the VRC−TST calculations, and the center-of-mass separation was found to be the optimum reaction coordinate. Furthermore, there was no indication of any reduction in the available phase space in the TS due to short-range repulsions. In essence, the absence of any repulsivity in the potential for separations of 4.1−8 Å coupled with the strength

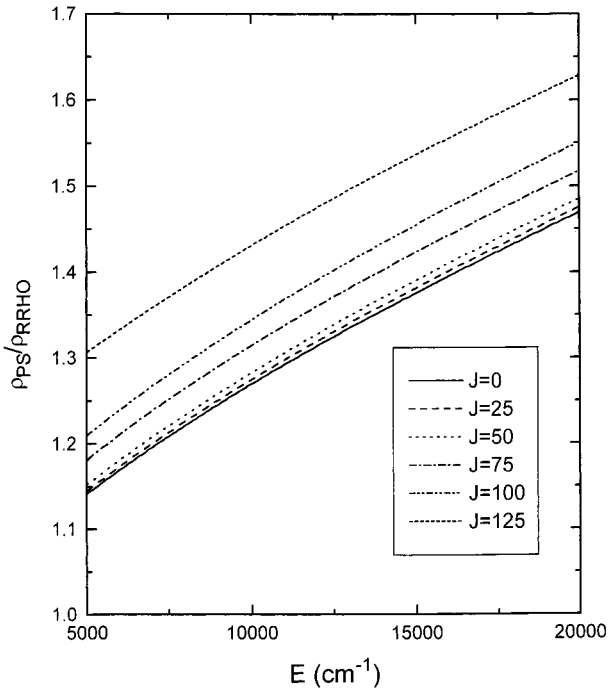

Figure 3. Plot of the ratio of the approximate quantum anharmonic nonrigid estimate for the density of states (eqs 2 and 3) to the quantum RRHO estimate as a function of energy for different values of the total angular momentum *J*. Note this plot is for the full density arising from the convolution of the conserved and transitional mode contributions.

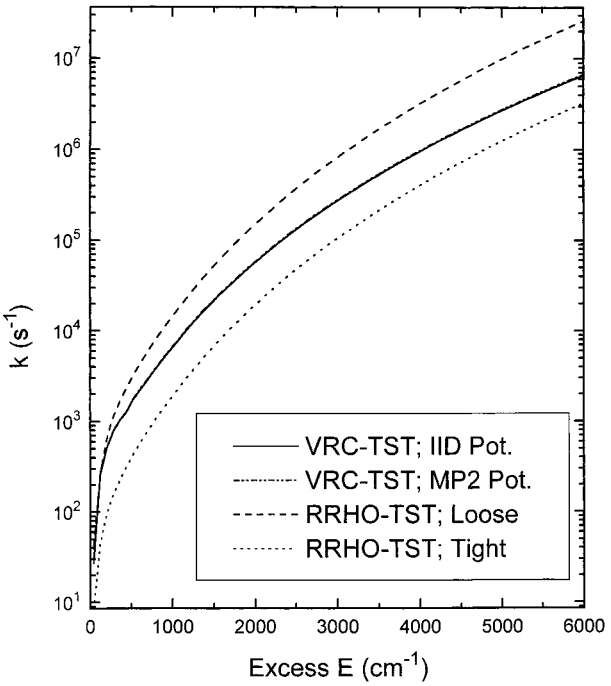

Figure 4. Plot of the various estimates for the dependence of the dissociation rate constants on excess energy. The solid line is the present VRC−TST estimate for the ion-induced dipole potential. The dot−dot−dashed line, which is obscured by the solid line, is the present VRC−TST estimate for the MP2 analytic potential. The dashed line and dotted line are for the loose and tight RRHO models of ref 5.

of the long-range attractions results in a TS which only lies at quite large separations.

Binding Energies from Kinetic Modeling. As discussed in detail by Armentrout and co-workers, the proper procedure for estimating the kinetic shift in the collision-induced dissociation experiments involves a convolution of the time scales for the dissociation process with various experimental time scales.[5] Here, we follow a somewhat simpler procedure which was found to reproduce the results obtained in ref 5 for the RRHO models. In particular, we evaluated the kinetic shift by determining that binding energy which provides a dissociation rate of $10^{3.5}$ s^{-1} for a total energy corresponding to the experimentally observed threshold energy E_0 and for the most probable J in a room temperature thermal distribution of reactants. The value of $10^{3.5}$ s^{-1} was chosen on the basis of its reproducing the results tabulated in ref 5 for the RRHO model and roughly corresponds to the experimental observation time scale of 10^{-4} s.

For the $Cr(C_6H_6)^+$ dissociation, the VRC−TST modeling of the collision-induced dissociation experiments yielded a binding energy of 40.5 kcal/mol compared with values of 40.6 and 39.2 kcal/mol for the loose and tight RRHO−TST models, respectively.[5] With no correction for the kinetic shift, the binding energy was estimated to be 42.5 kcal/mol. Thus, both the VRC−TST modeling and the loose RRHO−TST modeling predict a small kinetic shift of 1.9−2.0 kcal/mol, whereas the tight RRHO−TST modeling predicts a somewhat larger kinetic shift of 3.3 kcal/mol.

The kinetic modeling of the radiative association experiments according to the procedures outlined in ref 4 yields a binding energy of 43.6 kcal/mol. This value is somewhat larger than the value of 39.2 kcal/mol reported in ref 9 due to the larger metal−ligand vibrational frequencies and smaller radiative intensities for the dominant emitting modes in the present calculations.

The discrepancy of 3.1 kcal/mol between the collision-induced dissociation and radiative association values, while not large, is not as small as one might hope for. The extent of this discrepancy is perhaps an indication of the difficulty of accurately determining the contribution from the low-frequency ligand modes to ρ_{EJ}. Furthermore, for this particular molecule, the dependence of the estimated binding energy on the state density is somewhat stronger than usual due to the fact that one is approaching the high efficiency limit (i.e., the efficiency is 1.3%). As a result, a factor of 2 increase in the density of states decreases the estimated binding energy for the radiative association modeling by 1.8 kcal/mol. In contrast, this change would only decrease the collision-induced dissociation estimate by 0.5 kcal/mol. As mentioned in section IV, the strong dependence of the bending frequencies on the metal−ligand separation makes the accurate determination of these frequencies (or more precisely the state density) quite difficult.

Another possible source of error lies in the present overly simplified treatment of the energetic and angular momentum convolutions in the collision-induced dissociation experiments. Averages over the experimental time observation window may be performed as described by Armentrout and co-workers[1,2,5] and will be considered in future work. However, the smallness of the kinetic shift for this particular reaction, coupled with the sharpness of the rate energy curve, (cf. Figure 4) and the present reproduction of the tight transition-state model of ref 5, suggests that such errors should be quite small. More problematic is the uncertainty in the distributions of energy and, especially, angular momentum produced by the collisional excitation process, which might be expected to yield even greater errors in the final estimates. Finally, there may be errors in the estimated radiative emission rate or in either of the experimental data themselves.

It is interesting to consider how the loose and tight RRHO−TST predictions would vary if one implemented the present B3LYP estimates for the vibrational frequencies in place of the values from ref 5. What we find is that the RRHO−TST

predictions are nearly invariant to this correction. The explanation for this finding may be obtained by considering the particular TS models employed by Armentrout and co-workers.[5] In particular, the frequencies for the metal−ligand modes in the TS were taken to be proportional to the corresponding modes for the complex, and we have followed that assumption in repeating this RRHO−TST analysis. These metal−ligand frequencies are low enough that their contribution is near that expected on the basis of classical estimates. Thus, in taking the ratio of the transition state number of states to the complex density of states, the dependence on the absolute magnitude of the metal−ligand frequencies cancels.

In contrast, the VRC−TST estimates are strongly dependent on the frequencies employed for the complex since the effective metal−ligand frequencies for the TS are determined not by those for the complex but instead by the form of the metal−ligand interaction potential. Varying the metal−ligand frequencies for the complex then effects only the density of states for the complex and thus directly affects the dissociation rate constant. The fact that the loose TS and tight TS RRHO models of ref 5 span the VRC−TST results indicates that their choices for the ratio of the TS to complex frequencies were quite reasonable. These choices were based on the consideration of standard entropy changes, which in turn suggests that such standard entropy estimates are quite meaningful.

B. Dissociation Kinetics for other $M(C_6H_6)^+$. The kinetic modeling of the collision-induced dissociation for many of the other metal−benzene cations is complicated by the presence of multiple nearly degenerate electronic states for the metal ions. In this work, we consider two different limiting case assumptions in dealing with the effects of these degeneracies and near degeneracies. In particular, in one limiting case (g_{frag}) we assume that the transition state lies at such large separations that its electronic degeneracies and splittings are identical to those of the free metal ions. Furthermore, we assume that the electronic transitions rates are great enough to maintain a statistical distribution of their populations. The transition state number of states then includes a sum over the different electronic states of the fragments

$$N^{\dagger}_{\text{rovibronic}}(E, J) = \sum_i g_i N^{\dagger}_{\text{rovibrational}}(E - E_i, J) \qquad (4)$$

where g_i and E_i are the degeneracy and excitation energy of the ith electronic state. In the other limiting case (g_{comp}), we simply assume that the electronic degeneracy for the TS is equivalent to that for the complex. For both cases, the excited electronic states of the complexes are assumed to make no contribution to the density of states of the complex. The density of states for the complex is thus simply multiplied by the electronic degeneracy (spin and orbital) of its ground state.

Mn^+ and Cu^+. The lowest excited states of Mn^+ and Cu^+ are at least 1 eV above the ground state. Furthermore, one does not expect any low-lying excited states for the complex. Thus, just as for Cr^+, there is little uncertainty in the modeling for these compounds and one can expect quite satisfactory estimates for the kinetic shifts. The modeled binding energies for these and all the other metal−benzene cations are provided in Table 4 together with the prior modeling results from ref 5 and the current B3LYP DFT estimates. For Mn^+, the kinetic shift is estimated to be only 0.2 kcal/mol, which is smaller than that from both the loose and tight RRHO−TST models of ref 5. This result is expected for very small kinetic shifts since near the threshold the variational TS lies at large separations where the effective bending frequency is very low. For Cu^+, the kinetic shift is estimated to be 6.8 kcal/mol, which lies between the loose and tight values of 5.3 and 7.4, respectively. The kinetic shift for Cu^+ is relatively large due to the increased binding energy, which leads to an increased density of states for the complex at the dissociation threshold. Correspondingly, the dissociation rate is smaller at the threshold and a greater excess energy is required to produce a dissociation rate of $10^{3.5}$ s^{-1}. For species with even greater kinetic shifts, one would expect the VRC−TST kinetic shift to approach the tight TS value and perhaps even surpass it. For all three of these species, the VRC−TST modeled binding energies are in good agreement with the B3LYP quantum chemical binding energies, differing by no more than 2.4 kcal/mol.

TABLE 4: Binding Energies

metal	no kinetics[a]	loose[b]	tight[c]	VRC−TST[d]	B3LYP[e]
Ti	71.5	61.8	58.8	65.1(63.4)	56.9
				62.5(60.8)	
V	63.0	55.8	53.3	56.4(54.4)	49.7
Cr	42.5	40.6	39.2	40.5	38.9
Mn	32.3	31.8	31.4	32.1	34.5
^{4}Fe	54.2	49.6	47.5	49.9(49.0)	51.5
				44.4(43.5)	
Co	70.8	61.1	58.6	64.0(62.6)	61.2
Ni	66.0	58.1	55.8	58.0(57.5)	59.9
Cu	57.4	52.1	50.0	50.6	51.7

[a] Binding energy for modeling with no kinetic shift correction from ref 5. [b] Binding energy from ref 5 for loose RRHO−TST-based modeling of the kinetic shift. [c] Binding energy from ref 5 for tight RRHO−TST-based modeling of the kinetic shift. [d] Binding energy from present VRC−TST-based modeling of the kinetic shift. Primary values assume the electronic degeneracies and splittings of the TS equal those of the products. Numbers in parentheses assume an electronic degeneracy for the TS equal to that for the complex. The boldface values assume diabatic dynamics. [e] B3LYP quantum chemical estimate for the binding energy.

V^+, Co^+, and Ni^+. The lowest electronic states of V^+, Co^+, and Ni^+ are split by spin−orbit interactions, which result in a number of electronic states being accessible at the energies for which the dissociation is studied here. Furthermore, the states of the complex for V^+ and Ni^+ are orbitally degenerate. The confidence in the modeling is decreased by the uncertainty in the contribution from the excited spin−orbit states to the transition state number of states and, to a lesser extent, by the uncertainty in the contribution of excited states to the complex state density. The Jahn−Teller distortions may also increase the inaccuracies in the estimation of the density of states for the complex. The lowest spin−orbit excited states are at 36, 950, and 1507 cm^{-1} for V^+, Co^+, and Ni^+, respectively. Thus, these uncertainties are greatest for V^+, while for Co^+ and Ni^+ the statistical contributions from the excited spin−orbit states are actually negligible.

Comparisons of the kinetic shifts for the g_{comp} limiting case with the corresponding RRHO−TST results from ref 5 is probably most meaningful since this limiting case is likely to correspond with the assumptions made in ref 5. For this limiting case, the VRC−TST predictions for the kinetic shifts in these three ions are very similar, ranging from 8.2 to 8.6 kcal/mol. For the two Jahn−Teller-distorted species (V^+ and Ni^+), these kinetic shifts lie between the loose and tight RRHO−TST predictions. For the Co^+ species, the VRC−TST kinetic shift is actually 1.5 kcal/mol lower than that for the loose RRHO−TST prediction, which is somewhat surprising.

The VRC−TST-modeled binding energies for the Co^+ and Ni^+ species are both in reasonable agreement with the B3LYP quantum chemical results. The VRC−TST modeling results for the V^+ binding energy are somewhat (5−7 kcal/mol) higher

than the B3LYP estimate, which may simply be an indication of an underestimate in the B3LYP calculation.

Ti^+ and Fe^+. For Ti^+ and Fe^+ not only are there low-lying spin−orbit states (the lowest excited spin−orbit state of Ti^+ is at 94 cm^{-1} while that for Fe^+ is at 385 cm^{-1}), but the ground state of the complex requires a change in the electronic configuration from the ground state of the metal cation (from $d^{n-1}s$ to d^n). A key question for the modeling then involves the rate of transitions between these two electronic configurations. Unfortunately, such transition rates are not well-known, and so we again consider different limiting cases. An assumption of rapid transitions amongst these two configurations leads to the same two limiting cases as above. Alternatively, the g_{comp} and g_{frag} cases may be implemented for a diabatic framework, where there are no transitions between the two configurations. In these diabatic limiting cases, the ground-state to ground-state binding energy is then obtained by subtracting the excitation energy in the free metal ion from the modeling results.

It also probably worth noting that this electronic configuration switching probably leads to relatively low excitation energies for the first excited state of the complex. As a result, such excited electronic states may make an important contribution to the state density of the complex. For example, the sextet state of $Fe(C_6H_6)^+$ would appear to be only about 10 kcal/mol higher in energy than its ground quartet state. For these reasons, we consider the modeling of these two dissociations to be the most uncertain.

For Ti^+, the dissociation is likely to occur adiabatically to the ground-state ion since no spin transition is required. The VRC−TST adiabatically modeled binding energy is substantially higher than the B3LYP estimated energy but is in good agreement with the adjusted MCPF value from ref 6.

For Fe^+, the dissociation to ground-state ions requires a spin transition and so it is not clear whether it will occur diabatically or adiabatically. In this case, the adiabatic VRC−TST estimates employing the vibrational frequencies for the $3da_1^4 3da_2^1 3db_1^1 3db_2^1$ state agree reasonably well with both the B3LYP and MCPF quantum chemical binding energies. Employing the vibrational frequencies for the $3de_2^4 3da_1 3de_1^2$ state, which may actually be the ground state, results in a 2.0 kcal/mol increase in the modeled binding energies and even better agreement.

VI. Summary

The present VRC−TST-based kinetic modeling provides estimated metal−benzene cation binding energies which are in good agreement with B3LYP density functional theory calculations (i.e., discrepancies of ≤2 kcal/mol) for all but the Ti^+ and V^+ cases. For all but the Ti^+ and Fe^+ cases the variations in the limiting cases for the VRC−TST modeling are ≤2 kcal/mol. The kinetic shifts predicted by the VRC−TST modeling are generally in the range of the loose and tight RRHO−TST models of ref 5. For very small kinetic shifts the VRC−TST predictions are lower than the corresponding loose RRHO−TST. Then as the kinetic shift increases, the VRC−TST values first approach and then pass the loose RRHO−TST values, ultimately approaching the tight RRHO−TST values.

The modeling of the Cr^+ collision-induced dissociation and radiative association experiments is reasonably consistent, providing binding energies that differ by 3.1 kcal/mol. The remaining discrepancy may be an indication of the difficulties of accurately determining the potential energies for the metal−ligand vibrational modes. Alternatively, it may be necessary to implement improved models of the collision-induced dissociation process and/or to obtain improved radiative emission rates. The implementation of the full MP2-based analytic potential yielded negligible differences in the number of available states at the transition state. Furthermore, the density of the states for the complex was estimated to be only about 40% greater than the harmonic density for typical energies and total angular momentum.

Armentrout and co-workers have also examined the binding energies for the dimer complexes of benzene with the first-row transition-metal cations.[5] The kinetic shifts for these dimers are generally larger (the largest is 23 kcal/mol) and perhaps more importantly much more uncertain. Thus, in a companion study we have applied a roughly equivalent model in the estimation of binding energies for these dimers.[28]

Acknowledgment. The support of the National Science Foundation (CHE-9423725) and of the donors of the Petroleum Research Fund, adminstered by the American Chemical Society, is gratefully acknowledged.

Appendix

The classical density of states for the transitional modes may generally be written as

$$\rho(E,J) = \frac{\pi\hbar^3(2J+1)^2}{h^{N_t}} \int d\mathbf{q}_t\, d\mathbf{p}_t\, \delta(E - H_t)\delta[\mathbf{J}\hbar - \mathbf{J_t}(\mathbf{q}_t, \mathbf{p}_t)] \quad \text{(A1)}$$

where $\mathbf{q}_t$ and $\mathbf{p}_t$ are the coordinates and conjugate momenta for the transitional modes and H_t and $\mathbf{J_t}$ are the corresponding transitional mode Hamiltonian and angular momentum vector, respectively. Spatial symmetry was employed in writing eq A1, which allows for the consideration of a specific angular momentum vector **J** such as (0,0,J).

The transitional mode coordinates are represented here as the spherical polar coordinates $(R,\theta_{12},\phi_{12})$ for the separation and absolute orientation of the line connecting the centers-of-mass and the Euler angle coordinates $\Omega_i \equiv (\theta_i,\phi_i,\psi_i)$ defining the absolute orientation in space of each of the fragments. N_t is then the total number of such coordinates which amounts to 6 for the present case where the two fragments are an atom and a nonlinear rotor.

For a given value of the coordinates, the momenta in eq A1 may be integrated over analytically. Useful sample results for such analytic integrations are given in ref 29, where the emphasis was on procedures for the random sampling of the momenta. For the specific case provided by eq A1 one obtains

$$\rho(E,J) = \frac{(2J+1)^2}{4\pi h^{N_t-3}\Gamma[(N_t-3)/2]} \int d\mathbf{q}_t \frac{1}{|\mathbf{G}_t\cdot\mathbf{I}|^{1/2}} \times [2\pi(E - V_t - E_{rot})]^{(N_t-5)/2} \quad \text{(A2)}$$

where $|\mathbf{I}|$ is the determinant of the instantaneous moment of inertia tensor **I**, E_{rot} is the instantaneous rotational energy given by $\mathbf{J}\mathbf{I}^{-1}\mathbf{J}\hbar^2/2$, V_t is the transitional mode potential, and Γ is the gamma function. For the above choice of coordinates and two nonlinear fragments, the determinant of the transitional mode *G*-matrix is specified by

$$|\mathbf{G}_t|^{-1/2} = \mu_{12}^{1/2} I_{12} \sin\theta_{12} \left(\prod_{i=1}^{2} \sin\theta_i \prod_{j=1}^{3} I_{ij}^{1/2}\right) \quad \text{(A3)}$$

where μ_{12} and I_{12} are the effective mass and moments of inertia for the effective diatomic connecting the centers-of-mass of the

two fragments while I_{ij} is the jth component of the moment of inertia for the ith fragment. For an atomic fragment one simply drops the sin θ term and the moments of inertia for that fragment. Similarly, for a linear fragment one simply replaces the product over the three moments of inertia with a product over its two moments of inertia.

The validity of this general result may also be demonstrated via comparison with the phase-space volumes described in ref 30 where the emphasis was on the number of available states in the transition-state region. In particular, differentiation of eq 46 for Φ in ref 30 with respect to energy to convert from a number to a density yields the appropriate factor for integration over the momentum within a constant total angular momentum representation.

A crude Monte Carlo based evaluation of the integral in eq A3 provides an efficient and easily programmed means to evaluate the effect of anharmonicities on the density of states. In particular, random samplings of R within a box from $R_{\min}$ to $R_{\max}$, together with random samplings of cos θ_{12} and cos θ_i from -1 to 1, and of ϕ_i and ψ_i from 0 to 2π allows one to evaluate ρ_{EJ} as

$$\rho_{EJ} = \frac{2^{n_1+n_2}\,\pi^{n_1'+n_2'}\,(2J+1)^2(R_{\max}-R_{\min})\mu_{12}^{1/2}(\Pi_{i,j}I_{ij})^{1/2}}{h^{N_t-3}\gamma[(N_t-3)/2]K}\sum_{k=1}^{K} f_k \tag{A4}$$

where n_i is the number of rotational degrees of freedom for fragment i, $n_i' = \max(0, n_i - 1)$, f_k is essentially the coordinate dependent part of the integrand for a given set of coordinates $\mathbf{q}_{t_k}$

$$f_k = \left(\frac{I_{12}(\mathbf{q}_{t_k})}{|\mathbf{I}(\mathbf{q}_{t_k})|^{1/2}}\right)\{2\pi[E - V_t(\mathbf{q}_{t_k}) - E_{\mathrm{rot}}(\mathbf{q}_{t_k})]\}^{(N_t-5)/2} \tag{A5}$$

and K is the total number of random samplings.

For the present $Cr(C_6H_6)^+$ case, eq A4 reduces to

$$\rho_{EJ} = \frac{2^{3/2}}{K\pi\hbar^3}(2J+1)^2(R_{\max}-R_{\min})\mu_{C_6H_6,Cr}^{1/2} \times (I_{C_6H_6,x}I_{C_6H_6,y}I_{C_6H_6,z})^{1/2}\sum_{k=1}^{K}\left(\frac{I_{C_6H_6,Cr}(\mathbf{q}_{t_k})}{|\mathbf{I}(\mathbf{q}_{t_k})|^{1/2}}\right) \times \{2\pi[E - V_t(\mathbf{q}_{t_k}) - E_{\mathrm{rot}}(\mathbf{q}_{t_k})]\}^{1/2} \tag{A6}$$

Implementing the analytical potential for the interaction of benzene with Cr^+ in the evaluation of eq A6 then provides the classical anharmonic density of states $\rho_t^{c,a}$ for use in eq 3. Note that this procedure corrects for the effects of both anharmonicity and nonrigidity for these transitional modes.

Sample evaluations indicated that $R_{\min}$ and $R_{\max}$ values of 1.5 and 9 Å provided appropriate radial integration ranges with little variation for extensions to moderately larger separations for energies near the dissociation threshold. A total of 1×10^6 transitional-mode configurations were employed in the Monte Carlo evaluations of eq A6. In comparing with the classical harmonic estimates, a symmetry correction factor of $^1/_2$ was applied to these phase-space integral results to account for the inclusion of both faces of the bonding in the phase-space integral estimates.

References and Notes

(1) Schultz, R. H.; Crellin, K. C.; Armentrout, P. B. *J. Am. Chem. Soc.* **1991**, *113*, 8590. Khan, F. A.; Clemmer, D. E.; Schulz, R. H.; Armentrout, P. B. *J. Phys. Chem.* **1993**, *97*, 7978.

(2) Rodgers, M. T.; Ervin, K. M.; Armentrout, P. B. *J. Chem. Phys.* **1997**, *106*, 4499.

(3) Dunbar, R. C. *Int. J. Mass Spectrom.* **1990**, *100*, 423. Herbst, E.; Dunbar, R. C. *Mon. Not. R. Astron. Soc.* **1991**, *253*, 341. Dunbar, R. C. *Int. J. Mass Spectrom.* **1997**, *160*, 1.

(4) Klippenstein, S. J.; Yang, Y.-C.; Ryzhov, V.; Dunbar, R. C. *J. Chem. Phys.* **1996**, *104*, 4502.

(5) Meyer, F.; Khan, F. A.; Armentrout, P. B. *J. Am. Chem. Soc.* **1995**, *117*, 9740.

(6) Bauschlicher, C. W., Jr.; Partridge, H.; Langhoff, S. R. *J. Phys. Chem.* **1992**, *96*, 3273.

(7) Ouhlal, A.; Selmani, A.; Yelon, A. *Chem. Phys. Lett.* **1995**, *243*, 269.

(8) Lin, C.-Y.; Chen, Q. C.; Chen, H.; Freiser, B. S. *J. Phys. Chem. A* **1997**, *101*, 6023.

(9) Lin, C.-Y.; Dunbar, R. C. *Organometallics* **1996**, *16*, 2691.

(10) Becke, A. D. *J. Chem. Phys.* **1993**, *98*, 5648.

(11) Frisch, M. J.; Trucks, G. W.; Schlegel, H. B.; Gill, P. M. W.; Johnson, B. G.; Robb, M. A.; Cheeseman, J. R.; Keith, T.; Petersson, G. A.; Montgomery, J. A.; Raghavachari, K.; Al-Laham, M. A.; Zakrzewski, V. G.; Ortiz, J. V.; Foresman, J. B.; Cioslowski, J.; Stefanov, B. B.; Nanayakkara, A.; Challacombe, M.; Peng, C. Y.; Ayala, P. Y.; Chen, W.; Wong, M. W.; Andres, J. L.; Replogle, E. S.; Gomperts, R.; Martin, R. L.; Fox, D. J.; Binkley, J. S.; Defrees, D. J.; Baker, J.; Stewart, J. J. P.; Head-Gordon, M.; Gonzalez, C.; Pople, J. A. *GAUSSIAN 94*, Revision C.3; Gaussian Inc.: Pittsburgh, PA, 1995.

(12) Xantheas, S. S. *J. Chem. Phys.* **1996**, *104*, 8821.

(13) Møller, C.; Plesset, M. S. *Phys. Rev.* **1934**, *46*, 618. Pople, J. A.; Binkley, J. S.; Seeger, R. *Int. J. Quantum Chem. Symp.* **1976**, *10*, 1.

(14) Klippenstein, S. J. *J. Phys. Chem.* **1994**, *98*, 11459.

(15) Beyer, T.; Swinehart, D. F. *Commun. ACM* **1973**, *16*, 379. Stein, S. E.; Rabinovitch, B. S. *J. Chem. Phys.* **1973**, *58*, 2438.

(16) Bogaard, M. P.; Buckingham, A. D.; Pierens, R. K.; White, A. H. *J. Chem. Soc., Faraday Trans. 1* **1978**, *74*, 3008.

(17) Dennis, G. R.; Ritchie, G. L. D. *J. Phys. Chem.* **1991**, *95*, 656.

(18) Klippenstein, S. J. *Chem. Phys. Lett.* **1990**, *170*, 71, *J. Chem. Phys.* **1991**, *94*, 6469; **1992**, *96*, 367.

(19) Doll, J. D. *Chem. Phys. Lett.* **1980**, *72*, 139.

(20) Hase, W. L. In *Potential Energy Surfaces and Dynamics Calculations*; Truhlar, D. G., Ed.; Plenum Press: New York, 1981; p 1.

(21) Bhuiyan, L. B.; Hase, W. L. *J. Chem. Phys.* **1983**, *78*, 5052.

(22) Peslherbe, G. H.; Wang, H.; Hase, W. L. *J. Chem. Phys.* **1995**, *102*, 5626.

(23) Walch, S. P.; Bauschlicher, C. W. *J. Chem. Phys.* **1983**, *78*, 4597.

(24) Moore, C. E. *Atomic Energy Levels; As Derived from the Analysis of Optical Spectra*: U.S. National Bureau of Standards (U.S.) Circular No. 467; Vol. I, 1949; Vol. II, 1952.

(25) Klippenstein, S. J. Unpublished results.

(26) Ho, Y.-P.; Yang, Y.-C.; Klippenstein, S. J.; Dunbar, R. C. *J. Phys. Chem. A* **1997**, *101*, 3338.

(27) Waage, E. V.; Rabinovitch, B. S. *Chem. Rev.* **1970**, *70*, 377.

(28) Klippenstein, S. J.; Yang, C.-N. Manuscript in preparation.

(29) Randrup, J. *Comp. Phys. Comm.* **1990**, *59*, 439.

(30) Smith, S. C. *J. Chem. Phys.* **1992**, *97*, 2406.